Published OnlineFirst November 14, 2012; DOI: 10.1158/0008-5472.CAN-12-1888

Cancer Research

Histone Deacetylase Inhibitor AR-42 Differentially Affects Cell-cycle Transit in Meningeal and Meningioma Cells, Potently Inhibiting NF2-Deficient Meningioma Growth

Sarah S. Burns, Elena M. Akhmametyeva, Janet L. Oblinger, et al.

Cancer Res 2013;73:792-803. Published OnlineFirst November 14, 2012.

Published OnlineFirst November 14, 2012; DOI: 10.1158/0008-5472.CAN-12-1888

Therapeutics, Targets, and Chemical Biology

Cancer Research

Histone Deacetylase Inhibitor AR-42 Differentially Affects Cell-cycle Transit in Meningeal and Meningioma Cells, Potently Inhibiting *NF2*-Deficient Meningioma Growth

Sarah S. Burns[1,2], Elena M. Akhmametyeva[1,3], Janet L. Oblinger[1,2], Matthew L. Bush[2], Jie Huang[1,3], Volker Senner[5], Ching-Shih Chen[4], Abraham Jacob[2], D. Bradley Welling[2], and Long-Sheng Chang[1,2,3]

Abstract

Meningiomas constitute about 34% of primary intracranial tumors and are associated with increased mortality in patients with neurofibromatosis type 2 (NF2). To evaluate potential medical therapies for these tumors, we have established a quantifiable orthotopic model for *NF2*-deficient meningiomas. We showed that telomerase-immortalized Ben-Men-1 benign meningioma cells harbored a single nucleotide deletion in *NF2* exon 7 and did not express the *NF2* protein, merlin. We also showed that AR-42, a pan-histone deacetylase inhibitor, inhibited proliferation of both Ben-Men-1 and normal meningeal cells by increasing expression of $p16^{INK4A}$, $p21^{CIP1/WAF1}$, and $p27^{KIP1}$. In addition, AR-42 increased proapoptotic Bim expression and decreased anti-apoptotic Bcl_{XL} levels. However, AR-42 predominantly arrested Ben-Men-1 cells at G_2–M whereas it induced cell-cycle arrest at G_1 in meningeal cells. Consistently, AR-42 substantially decreased the levels of cyclin D1, E, and A, and proliferating cell nuclear antigen in meningeal cells while significantly reducing the expression of cyclin B, important for progression through G_2, in Ben-Men-1 cells. In addition, AR-42 decreased Aurora A and B expression. To compare the *in vivo* efficacies of AR-42 and AR-12, a PDK1 inhibitor, we generated and used luciferase-expressing Ben-Men-1-LucB cells to establish intracranial xenografts that grew over time. While AR-12 treatment moderately slowed tumor growth, AR-42 caused regression of Ben-Men-1-LucB tumors. Importantly, AR-42–treated tumors showed minimal regrowth when xenograft-bearing mice were switched to normal diet. Together, these results suggest that AR-42 is a potential therapy for meningiomas. The differential effect of AR-42 on cell-cycle progression of normal meningeal and meningioma cells may have implications for why AR-42 is well-tolerated while it potently inhibits tumor growth. *Cancer Res; 73(2); 792–803. ©2012 AACR.*

Introduction

Meningiomas are tumors originating from the meningothelial cells of the arachnoid layer lining the brain and can occur at the convexity, the skull base, and along the spine (1). About 80% of meningiomas are benign (WHO grade I), whereas the remaining are atypical (grade II) and anaplastic (grade III). These tumors cause significant morbidity, including cranial nerve palsy, seizures, and brainstem compression, which may lead to paralysis, aspiration pneumonia, and death. Surgical resection and radiation are current treatment options; however, complete resection of tumors is often difficult, especially for those located along the skull base. Approximately 20% of benign meningiomas recur over 10 years, whereas grade II and grade III tumors possess greater rates of recurrence. Meningiomas can occur sporadically or in patients with neurofibromatosis type 2 (NF2), a genetic disorder characterized by the development of multiple nervous system tumors, including meningiomas and vestibular schwannomas (2). Meningiomas in patients with NF2 are associated with disease severity and increased risk of mortality. Patients with NF2 often have multiple tumors, and their treatment is challenging. Consequently, the development of novel and effective medical therapeutics to treat meningiomas is urgently needed.

NF2 is caused by mutations in the *Neurofibromatosis 2* (*NF2*) gene, which encodes the tumor suppressor protein merlin (3, 4). Most NF2-associated meningiomas and about 50% to 60% of sporadic meningiomas contain *NF2* mutations (2). The observation that *NF2* mutations are present in both benign and malignant meningiomas suggests that *NF2* inactivation may be an early tumorigenic event and that loss of merlin disrupts

Authors' Affiliations: [1]Center for Childhood Cancer, The Research Institute at Nationwide Children's Hospital; Departments of [2]Otolaryngology and [3]Pediatrics, The Ohio State University College of Medicine; [4]The Ohio State University College of Pharmacy, Columbus, Ohio; and [5]Institut für Neuropathologie Universitätsklinikum Münster, Germany

Note: Supplementary data for this article are available at Cancer Research Online (http://cancerres.aacrjournals.org/).

Current address for M.L. Bush: Department of Otolaryngology-Head and Neck Surgery, The University of Kentucky, Lexington, Kentucky; and current address for A. Jacob: Department of Surgery, Division of Otolaryngology-Head and Neck Surgery, University of Arizona, Tucson, Arizona.

Corresponding Author: Long-Sheng Chang, Center for Childhood Cancer, The Research Institute at Nationwide Children's Hospital, Columbus, OH 43205. Phone: 614-355-2658; Fax: 614-722-5895; E-mail: lchang@chi.osu.edu

doi: 10.1158/0008-5472.CAN-12-1888

Published OnlineFirst November 14, 2012; DOI: 10.1158/0008-5472.CAN-12-1888

important signaling pathways, ultimately leading to tumorigenesis. Merlin-deficient meningioma cells exhibit specific characteristics, such as cytoskeletal and cell contact defects, altered cell morphology and growth properties, and susceptibility to senescence (5). In addition, *Nf2* inactivation in arachnoidal cells or meningeal precursor cells leads to meningioma formation in mice, further corroborating the role of merlin in tumorigenesis (6, 7). While these mouse models await further characterization, additional models that closely mimic the clinical presentation of *NF2*-deficient benign meningiomas and facilitate efficient quantitation of intracranial tumor growth will enhance therapeutic testing.

Meningioma cell lines are valuable tools to study tumor biology and potential treatments. Several patient-derived cell lines, such as IOMM-Lee and KT21-MG1, have been established from malignant meningiomas, which exhibit complex genetic changes and aggressive features (8–10). Using IOMM-Lee cells and primary meningioma cultures, McCutcheon and colleagues (11) generated orthotopic xenografts; however, tumor growth was not monitored over time, and primary meningioma cells did not uniformly produce tumors. Baia and colleagues (12) established intracranial xenografts with luciferase-expressing IOMM-Lee cells and used bioluminescence imaging (BLI) to quantify tumor growth. However, a quantifiable *NF2*-deficient, benign meningioma model has not been described. While several benign meningioma cell lines have been developed using the HPV E6/E7 or SV40 T-antigen (13, 14), transformation by viral oncogenes alters growth signaling and behavior of these cells. Püttmann and colleagues (15) generated a benign meningioma cell line, Ben-Men-1, from a grade I meningioma using telomerase. Ben-Men-1 cells exhibit characteristics of meningothelial differentiation and lack one copy of chromosome 22, which harbors the *NF2* gene. However, the status of the second *NF2* allele in Ben-Men-1 cells is not known.

NF2 inactivation in meningiomas and vestibular schwannomas perturbs several signaling pathways, including the AKT pathway (16–20). Previously, we showed that a small-molecule inhibitor of the AKT pathway, AR-12 (formerly OSU-03012), effectively inhibits the growth of *NF2*-deficient schwannoma cells (21). We also showed that AR-42 (HDAC-42), a pan-histone deacetylase inhibitor (HDACi), potently inhibits schwannoma and meningioma cell proliferation (22, 23). In addition to inhibiting the activities of histone deacetylases, which are frequently overexpressed in human cancers (24), AR-42 can also reduce AKT phosphorylation by disrupting the interaction between HDAC6 and protein phosphatase-1 (PP1), enabling free PP1 to dephosphorylate AKT (25). However, the efficacies of these compounds have not been evaluated in an *NF2*-deficient, benign meningioma model *in vivo*. Furthermore, the effect of AR-42 in normal meningeal cells has not been examined.

Here, we showed that Ben-Men-1 cells are *NF2*-deficient. Using luciferase-expressing Ben-Men-1 cells, we established a quantifiable intracranial meningioma model to evaluate AR-42 and AR-12 as potential therapies. Also, we found that AR-42 differentially inhibited cell-cycle progression of normal meningeal and meningioma cells.

Materials and Methods

Cell cultures and drugs

Ben-Men-1 benign meningioma cells have been described (15). Malignant meningioma KT21-MG1 and IOMM-Lee cells (8, 9) were kindly provided by Dr. Anita Lal, University of California, San Francisco (San Francisco, CA). HE1-1 is an adenovirus E1-transformed human embryonic kidney cell line (unpublished), and HMS-97 is a human malignant schwannoma cell line (26). All cell lines and primary human meningeal cells (ScienCell) were grown in Dulbecco's Modified Eagle Medium with 10% FBS (Invitrogen). AR-42 and AR-12 were supplied by Arno Therapeutics and formulated into rodent chow (Research Diets) to deliver about 25 and 100 mg/kg/d, respectively (21–23). Also, AR-42 was dissolved in dimethyl sulfoxide (DMSO) for *in vitro* experiments.

Mutational analysis

Genomic DNA was extracted from Ben-Men-1 cells using the PureGene DNA Isolation Kit (Qiagen). *NF2* exons were amplified by PCR using Takara ExTaq DNA polymerase and primer pairs flanking each exon (27). PCR products were purified using the Qiagen Gel Extraction kit and sequenced from both 5′- and 3′-directions via automated DNA sequencing. The results were confirmed by sequencing PCR products obtained using PfuUltra High-fidelity DNA polymerase (Stratagene).

Cell proliferation assay and flow cytometry

Cells were plated at 7,500 cells per well in 96-well plates overnight and treated with various concentrations of AR-42 for 72 hours. Cell proliferation was measured by resazurin assay (28), and the 50% inhibitory concentration (IC_{50}) was calculated (21). For cell-cycle analysis, subconfluent cells were treated with 1 μmol/L AR-42 or DMSO as a control for 2 days. For mitotic block, nocodazole (100 ng/mL) was added to drug-treated cells for another 24 hours before harvesting. Following treatment, floating and adherent cells were collected, washed, and fixed in 75% ethanol (29). Fixed cells were incubated with 0.2 mol/L phosphate-citrate buffer, pH 7.8, to extract low-molecular-weight DNA, stained in propidium iodide (50 μg/mL) and RNase A (100 μg/mL), and analyzed using a Calibur fluorescence-activated cell sorter (Becton Dickinson; ref. 29). Data analysis was conducted using FlowJo software (TreeStar).

Western blot

Subconfluent cells were treated with the indicated concentrations of AR-42 for 1 or 2 days. Treated cells were harvested and lysed in cold radioimmunoprecipitation assay (RIPA) buffer supplemented with protease inhibitor cocktail (Sigma). Equal amount of protein (20 μg) in each lysate was run on an SDS-polyacrylamide gel, and Western blot analysis was conducted as described previously (21).

Lentiviral transduction

Ben-Men-1 cells were transduced with Lenti-CMV-Luc lentiviruses (Qiagen) in the presence of hexadimethrine bromide (8 μg/mL) at 37°C overnight. Transduced cells were passaged at 1:5 dilution and then selected for puromycin resistance. Luciferase activity was detected using the Luciferase Reporter

Published OnlineFirst November 14, 2012; DOI: 10.1158/0008-5472.CAN-12-1888

Assay System (Promega; ref. 30), and the clone with the highest activity, designated Ben-Men-1-LucB (data not shown), was used subsequently.

Establishment of a skull-base meningioma model

The Institutional Animal Care and Use Committee at Nationwide Children's Hospital approved this animal study. Ben-Men-1-LucB cells were harvested, washed, and resuspended in PBS (0.5×10^6 to 1×10^6 cells/mouse in 3 μL). Six- to 8-week-old SCID C.B17 mice were anesthetized with 5% isoflurane (Baxter), and their heads were stabilized in a Kopf Small-Animal Stereotaxic Instrument. A midline sagittal incision was made on the cranial skin, and a burr hole was drilled in the skull 1.5 mm anterior and 1.5 mm to the right of the bregma. A 26-gauge needle attached to a 10-μL Hamilton syringe loaded with cells was slowly inserted through the burr hole and downward about 5 mm to the skull base. The cell suspension was injected at a rate of 1.5 μL/min via an automatic microinjection unit, and the needle was left in place for 1 minute before being withdrawn slowly. The incision was closed using 3 M VetBond Tissue Adhesive. After recovery, mice were monitored for tumor growth and any neurologic deficits.

BLI and small-animal MRI

To verify tumor establishment, mice stereotactically inoculated with Ben-Men-1-LucB cells were imaged using a Xenogen IVIS Spectrum (Caliper) 2 and 4 weeks after injection. Briefly, mice were injected intraperitoneally with D-luciferin (150 mg/kg body weight; Caliper) and anesthetized with isoflurane. Kinetic analysis of luciferase activity was conducted to identify the time at which the peak luminescent signal was emitted. All subsequent BLI was conducted at this peak time. Once tumors had established, mice were divided into 3 groups and fed normal diet, AR-42–formulated diet, or AR-12–containing diet *ad libitum*. Tumor growth was monitored monthly by BLI. Photon emission was quantified by region of interest analysis using Living Image software (Caliper). Because of variation in initial tumor size, the luminescence for each mouse was normalized to the signal measured before treatment and expressed as the mean normalized luminescence ± SD for each treatment group ($n = 5$ per group). Also, photon emission from a representative group of mice measured together for each indicated time point was displayed as total flux. A cohort of mice treated with AR-42 for 6 months were switched to normal diet for an additional 6 months and imaged monthly to assess the extent of tumor regrowth.

For MRI, mice were anesthetized with isoflurane, injected intraperitoneally with Magnevist contrast agent (0.1 mmol/L/kg), and scanned using a BioSpec 94/30 USR 9.4 T microMRI (Bruker). Tumor volumes were calculated from T1 images as described previously (22, 26).

Immunohistochemistry

Mice were injected intraperitoneally with bromodeoxyuridine (BrdUrd; 0.5 mg per 10 g body weight) 2 hours before euthanasia. Heads were dissected and fixed in 10% phosphate-buffered formalin. Following washing in running water for 2 hours, heads were treated with 0.1 mol/L Tris-HCl, pH 7.2 overnight and decalcified in 0.35 mol/L EDTA in 0.1 mol/L Tris-HCl, pH 6.95 for 10 to 14 days. After optimal decalcification (31), samples were cut in half, incubated in 10% sucrose in 0.1 mol/L Tris-HCl, pH 7.2 overnight, and embedded in paraffin. Sections (5 μm) were obtained, deparaffinized, and stained with hematoxylin and eosin. For immunostaining, deparaffinized sections were heated in 1 mmol/L citric acid, pH 6.0, in a steamer for 20 minutes and sequentially treated with 3% hydrogen peroxide, Super Block, and a primary antibody overnight (Supplementary Methods), followed by incubation with a horseradish peroxidase (HRP)-conjugated secondary antibody and color development with AEC chromogen (ScyTek). Hematoxylin was used as a counterstain. Stained sections were mounted and visualized under a Zeiss Axioskop microscope. Negative controls were treated with the same procedure but without the primary antibody.

Results

Ben-Men-1 benign meningioma cells are *NF2*-deficient

As Ben-Men-1 cells lack one copy of chromosome 22, which contains the *NF2* gene (15), we determined the status of the remaining *NF2* allele by scanning the 17 *NF2* exons for mutations. We detected a deletion of a cytosine (nucleotide #640 relative to the major transcription initiation site designated as +1; ref. 30) in exon 7 in Ben-Men-1 cells, resulting in a premature stop codon 5 amino acids downstream of the mutation (Fig. 1A).

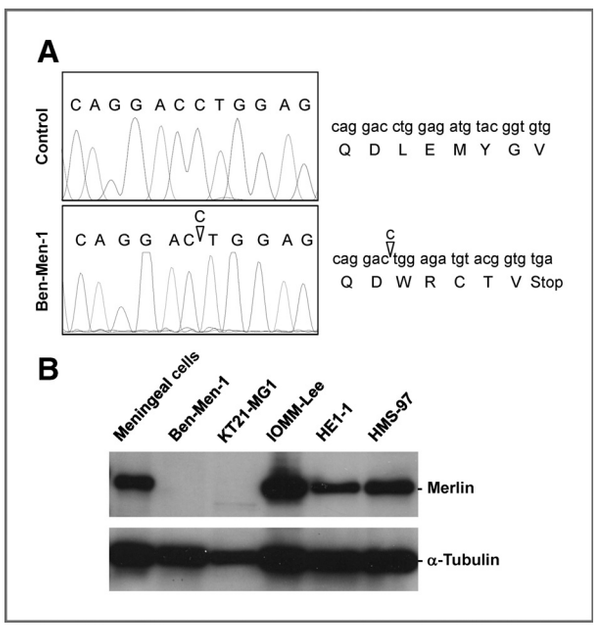

Figure 1. Ben-Men-1 cells contain a mutation in the *NF2* gene and do not express merlin. A, Ben-Men-1 cells carry a deletion of a cytosine residue (del640C; marked with an inverted triangle) in *NF2* exon 7, resulting in premature termination. The 17 *NF2* exons were obtained from Ben-Men-1 and control DNA by PCR and sequenced according to Materials and Methods. B, Western blot analysis showed that Ben-Men-1 benign meningioma cells and KT21-MG1 malignant meningioma cells did not express merlin protein, in contrast to normal meningeal cells, IOMM-Lee malignant meningioma cells, HE1-1 embryonic kidney cells, and HMS-97 malignant schwannoma cells. α-Tubulin was used as a loading control.

Published OnlineFirst November 14, 2012; DOI: 10.1158/0008-5472.CAN-12-1888

Western blot analysis revealed that Ben-Men-1 cells did not express merlin protein, in contrast to meningeal cells, IOMM-Lee malignant meningioma cells, and HMS-97 malignant schwannoma cells (Fig. 1B). While the frameshift mutation predicts a truncated product of 218 amino acids, a protein of this size was not detected in Ben-Men-1 cells (Supplementary Fig. S1). In addition, we did not detect merlin protein in KT21-MG1 malignant meningioma cells. These results indicate that Ben-Men-1 and KT21-MG1 cells are *NF2*-deficient.

AR-42 differentially affects cell-cycle progression of normal meningeal and Ben-Men-1 meningioma cells

Previously, we showed that AR-42 decreased Ben-Men-1 cell growth with an IC_{50} of about 1 μmol/L (22). Intriguingly, AR-42 also inhibited proliferation of meningeal cells at a similar IC_{50} (Supplementary Fig. S2). Consistent with its action as an HDACi (32), AR-42 treatment increased global acetylation of intracellular proteins, including histone H2B, in both meningeal and Ben-Men-1 cells (Supplementary Fig. S3A and S3B). Also, AR-42 decreased expression of p-AKT and 2 downstream targets of the AKT/mTOR pathway, p-S6 ribosomal protein and p-4E-BP1, in both cell types. These results indicate that AR-42 exerts similar effects on protein acetylation and the AKT pathway in meningeal and meningioma cells.

To compare the effect of AR-42 on cell-cycle progression, we conducted flow cytometric analysis on meningeal and Ben-Men-1 cells treated with 1 μmol/L AR-42 for 2 days. Consistent with our previous observation (22), AR-42 treatment substantially increased the number of Ben-Men-1 cells in G_2–M from 13.1% to 38.8% (Fig. 2). Intriguingly, AR-42 did not affect the percentage of meningeal cells in G_2–M but increased the G_1 population from 87.5% to 90%, suggesting G_1 arrest. To enhance detection of cells arrested in G1, nocodazole, an agent that disrupts microtubule polymerization, was added to AR-42-treated cells for another day (from 48 to 72 hours) to block cells in M phase. Note that the doubling time for Ben-Men-1 cells is about 2 days (15), and meningeal cells double about every 3 days (Supplementary Fig. S4). Addition of nocodazole to AR-42–treated meningeal cells significantly increased the G_1 population compared with the nocodazole/DMSO-treated control (from 83.1% to 89.1%; Fig. 2), confirming that AR-42 induced G_1 arrest in meningeal cells. As expected, nocodazole substantially increased the percentage of DMSO-treated Ben-Men-1 cells in G_2–M from 13.1% to 61.1% while decreasing the G_1 fraction from 72.6% to 18.2%. However, addition of nocodazole to AR-42–treated Ben-Men-1 cells only slightly increased the G_2–M population compared with AR-42–treated cells in the absence of nocodazole (from 38.8% to 40.2%), suggesting that AR-42 also impeded G_1 progression of Ben-Men-1 cells. Collectively, these results showed that AR-42 inhibited cell-cycle progression of Ben-Men-1 meningioma cells in both G_2–M and G_1, whereas it arrested meningeal cells in G_1.

AR-42 modulates the expression of cell-cycle regulators

To investigate the mechanism by which AR-42 differentially induces cell-cycle arrest in meningeal and Ben-Men-1 cells, we analyzed the expression of various cyclin-dependent kinase

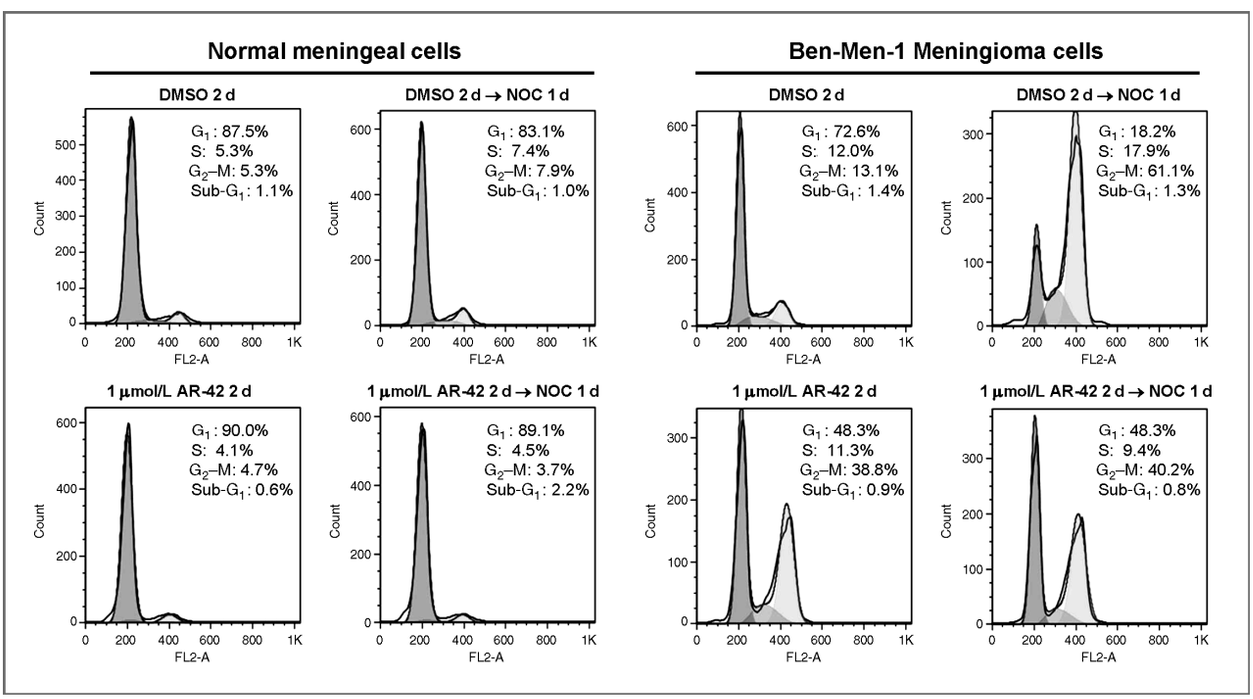

Figure 2. Differential effect of AR-42 on cell-cycle progression of normal meningeal and Ben-Men-1-LucB cells. Meningeal and Ben-Men-1-LucB cells were treated with 1 μmol/L AR-42 or DMSO for 2 days. To block cells in mitosis, nocodazole (NOC) was added to AR-42–treated cells for another day. After fixation, cells were stained with propidium iodide and analyzed by flow cytometry. AR-42 treatment increased the fraction of Ben-Men-1 cells in G_2–M, while increasing the number of meningeal cells in the G_1 population. Addition of nocodazole further increased the percentage of meningeal cells in G_1.

Published OnlineFirst November 14, 2012; DOI: 10.1158/0008-5472.CAN-12-1888

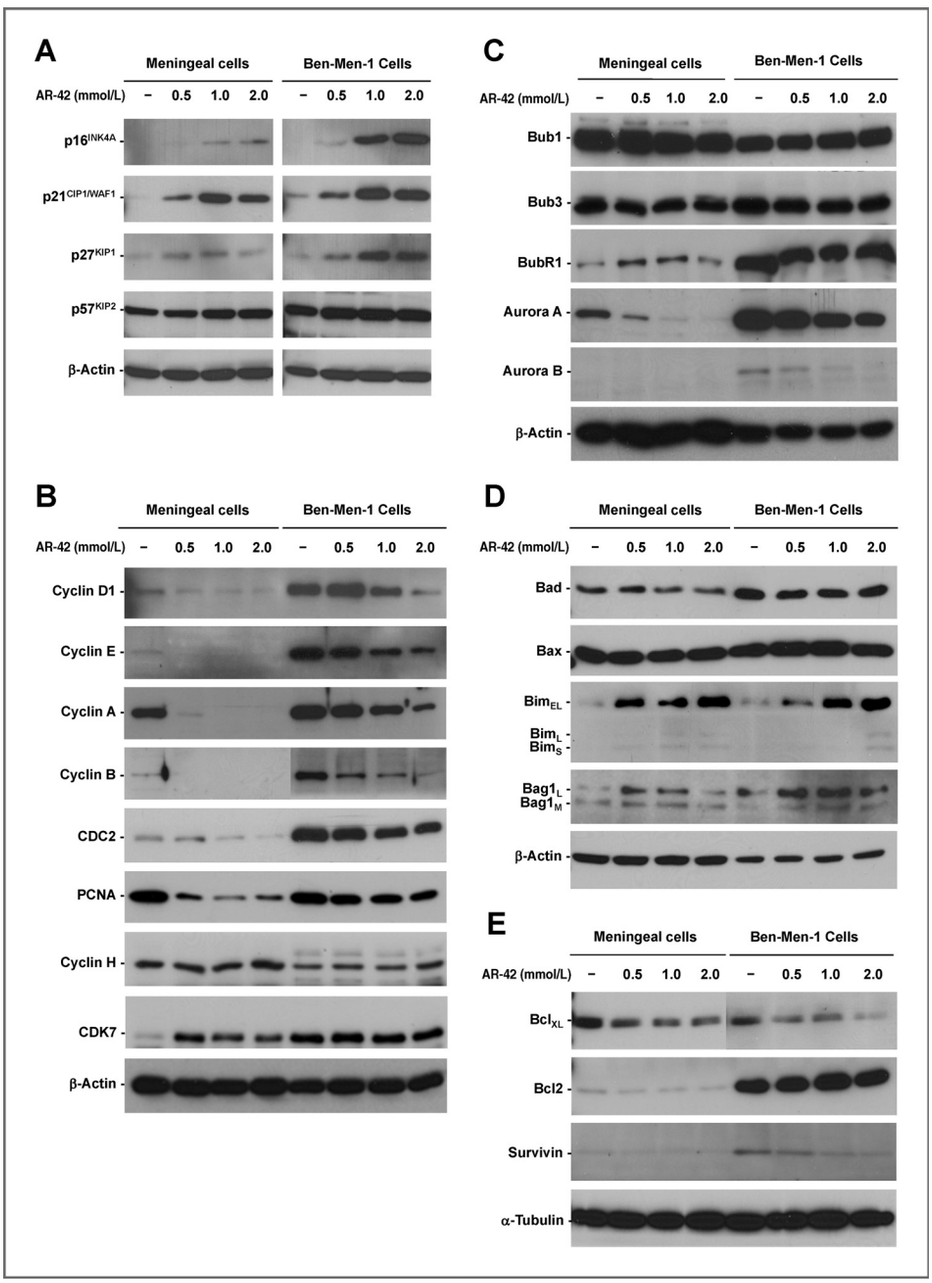

Figure 3. The effects of AR-42 on the expression of various cell-cycle and apoptotic regulators. Western blot analysis showed that the levels of $p16^{INK4A}$, $p21^{CIP1/WAF1}$, and $p27^{KIP1}$ increased in meningeal and Ben-Men-1 cells treated with AR-42 for 24 hours (A). While AR-42 attenuated the expression of cyclin D1, cyclin E, cyclin B, and CDC2, a marked reduction in the cyclin A and PCNA levels was observed in meningeal cells (B). However, AR-42 only modestly decreased PCNA expression but significantly reduced the cyclin B level in Ben-Men-1 cells. AR-42 decreased the levels of Aurora A and Aurora B, whereas Bub1, Bub3, and BubR1 expression were unaffected (C). AR-42 increased the expression of Bim isoforms (Bim_{EL}, Bim_L, and Bim_S) and Bag1 isoforms ($Bag1_L$ and $Bag1_M$; D), whereas decreasing the levels of Bcl_{XL} and survivin in meningeal and Ben-Men-1 cells (E). β-Actin and α-tubulin were used as loading controls.

(CDK) inhibitors and cyclins. Both meningeal and Ben-Men-1 cells expressed low levels of $p16^{INK4A}$, $p21^{CIP1/WAF1}$, and $p27^{KIP1}$. Treatment with AR-42 induced the expression of these CDK inhibitors in a dose-dependent manner in both cell types (Fig. 3A). However, AR-42 did not affect $p57^{KIP2}$ expression. These results show that inhibition of cell-cycle progression by AR-42 in meningeal and Ben-Men-1 cells is mediated, in part, by induction of multiple CDK inhibitors.

Mitogen stimulation induces the expression of cyclin D, which activates CDK4/6 at early G_1, followed by increasing cyclin E and A levels during late G_1. CDK2, which binds to cyclin E and A, and CDC2, which binds to cyclin E, promote the G_1–S transition. In addition, cyclin B and CDC2 are important for progression through G_2 (33). While Ben-Men-1 cells expressed higher basal levels of cyclin D1 and E than meningeal cells, AR-42 treatment attenuated the expression of these cyclins and markedly decreased the cyclin A level in meningeal cells (Fig. 3B). The decreased expression of these cyclins corroborated the observation that AR-42 induced G_1 arrest in meningeal cells. Consistently, AR-42 notably reduced the level of proliferating cell nuclear antigen (PCNA), a protein induced in S-phase, and further decreased cyclin B and CDC2 expression in meningeal cells. Similarly, AR-42 treatment lowered the expression of cyclin D1, E, and A in Ben-Men-1 cells, albeit

Published OnlineFirst November 14, 2012; DOI: 10.1158/0008-5472.CAN-12-1888

the decrease was less dramatic. Consistent with G_2–M arrest, AR-42 only modestly decreased PCNA expression but significantly reduced the cyclin B level in Ben-Men-1 cells.

Taken together, these results suggest that AR-42 differentially affects cell-cycle progression of normal meningeal and Ben-Men-1 meningioma cells by regulating the expression of various cyclins and CDK inhibitors.

AR-42 decreases the expression of Aurora kinases and modulates the levels of apoptotic factors

We also analyzed the effect of AR-42 on the expression of various mitotic spindle assembly checkpoint kinases (34). Both meningeal and Ben-Men-1 cells strongly expressed Bub1 and Bub3; however, Ben-Men-1 cells exhibited higher levels of BubR1, Aurora A, and Aurora B than meningeal cells (Fig. 3C). While the Bub1, Bub3, and BubR1 levels were not affected by AR-42 treatment, Aurora A expression decreased substantially in both meningeal and Ben-Men-1 cells treated with AR-42. Also, the level of Aurora B decreased in AR-42–treated Ben-Men-1 cells. The reduced expression of Aurora kinases may further reinforce the effect of AR-42 on G_2–M arrest in Ben-Men-1 cells.

AR-42 induces apoptosis in several types of tumor cells (22, 32, 35, 36); however, its effects on normal and tumor cells have not been compared. AR-42 treatment increased the expression of proapoptotic Bim in a dose-dependent manner but did not affect the levels of Bad and Bax in both meningeal and Ben-Men-1 cells (Fig. 3D). Similarly, AR-42 increased the Bag1 level; however, the increase was not as pronounced at higher concentrations (e.g., 2 μmol/L). Conversely, AR-42 decreased the expression of antiapoptotic Bcl_{XL} and survivin in both cell types (Fig. 3E). While Ben-Men-1 cells expressed higher levels of Bcl2 and survivin than in meningeal cells, the expression of Bcl2 was not affected by AR-42 treatment. These results indicate that AR-42 affects the expression of specific pro- and anti-apoptotic regulators.

AR-42 and AR-12 inhibited tumor growth in a quantifiable intracranial benign meningioma model

To establish a quantifiable model for *NF2*-deficient benign meningiomas, we stereotactically injected luciferase-expressing Ben-Men-1-LucB cells, which exhibited a similar sensitivity to AR-42 as their parental Ben-Men-1 cells (Supplementary Fig. S5), to the skull base of SCID mice and monitored tumor growth by BLI. Ben-Men-1-LucB tumors grew slowly over time (Fig. 4A). Unlike KT21-MG1 malignant meningioma xenografts, which invaded the brain tissue (Supplementary Fig. S6), Ben-Men-1-LucB tumors grew from the site of injection along the side of the brain (Fig. 4B). As in the original tumor, which expressed epithelial membrane antigen and vimentin, markers commonly used for meningiomas (15), we detected strong staining for vimentin in Ben-Men-1-LucB tumors (Supplementary Fig. S7). These results showed a quantifiable, orthotopic *NF2*-deficient benign meningioma model in which tumor growth could be easily monitored.

Using this model, we compared the *in vivo* efficacies of AR-42 and AR-12. Mice with established Ben-Men-1-LucB tumors were fed normal diet or diet containing AR-42 or AR-12 for 6 months. BLI showed that the tumors in mice fed normal diet

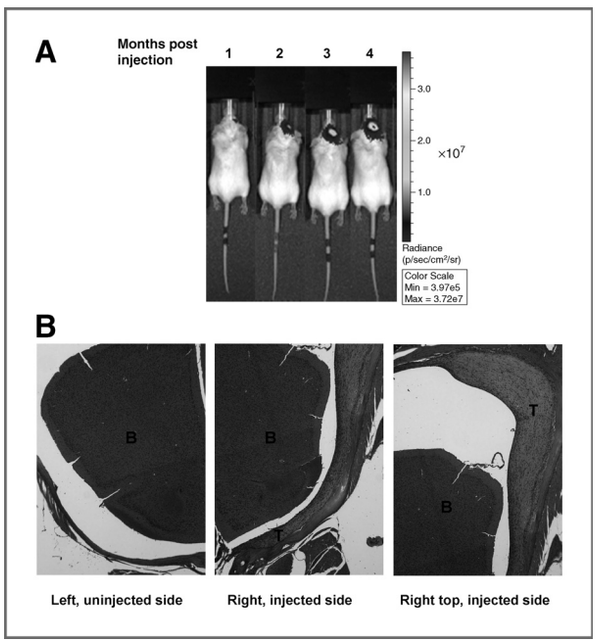

Figure 4. Ben-Men-1-LucB cells established intracranial xenograft tumors that grew slowly along the skull over time. A, about 5×10^5 Ben-Men-1-LucB cells were stereotactically injected at the skull base, and tumor growth was monitored by BLI according to Materials and Methods. BLI detected increased bioluminescent signal in Ben-Men-1-LucB xenograft–bearing mice with each month after injection. B, hematoxylin and eosin staining of the head region of a xenograft-bearing mouse 4 months after implantation showed that Ben-Men-1-LucB tumors grew from the site of injection along the skull to the top of the head region and did not invade the adjacent brain tissue. B, brain; T, tumor.

grew steadily as shown by an increase in bioluminescence signal over time (Fig. 5A; Supplementary Fig. S8A and S8B). The tumors in mice fed AR-12 diet also continued to increase in size; however, the growth was slower than those in mice fed normal diet by an average of about 54% after 6 months of treatment (Supplementary Fig. S8B). In contrast, the tumors in mice fed AR-42 regressed, as evident by a sharp decrease in bioluminescence signal after 1 month, and remained small in subsequent months (Fig. 5A and 5B). AR-42 treatment reduced the bioluminescence signal by ~82% (avg.) after 1 month and about 92% after 6 months (Fig. 5B).

MRI confirmed inhibition of tumor growth by AR-42 and AR-12. While tumors were observed in mice fed normal diet and AR-12-containing chow, the tumor volumes in AR-12-treated mice were smaller than those in mice fed normal diet (Fig. 5C; Supplementary Table S1). In contrast, tumors were not detected in mice treated with AR-42 for 4 to 6 months. A small tumor was found in a mouse treated with AR-42 for a shorter duration (Supplementary Fig. S9). It should be noted that the BLI detected a greater attenuation of tumor growth in AR-12–treated mice (compared with normal diet) than MRI (Supplementary Table S1). Nonetheless, both methods confirmed that AR-12 attenuated tumor growth.

Collectively, these results indicate that AR-42 causes tumor regression, whereas AR-12 moderately slows the growth of tumors over time.

Published OnlineFirst November 14, 2012; DOI: 10.1158/0008-5472.CAN-12-1888

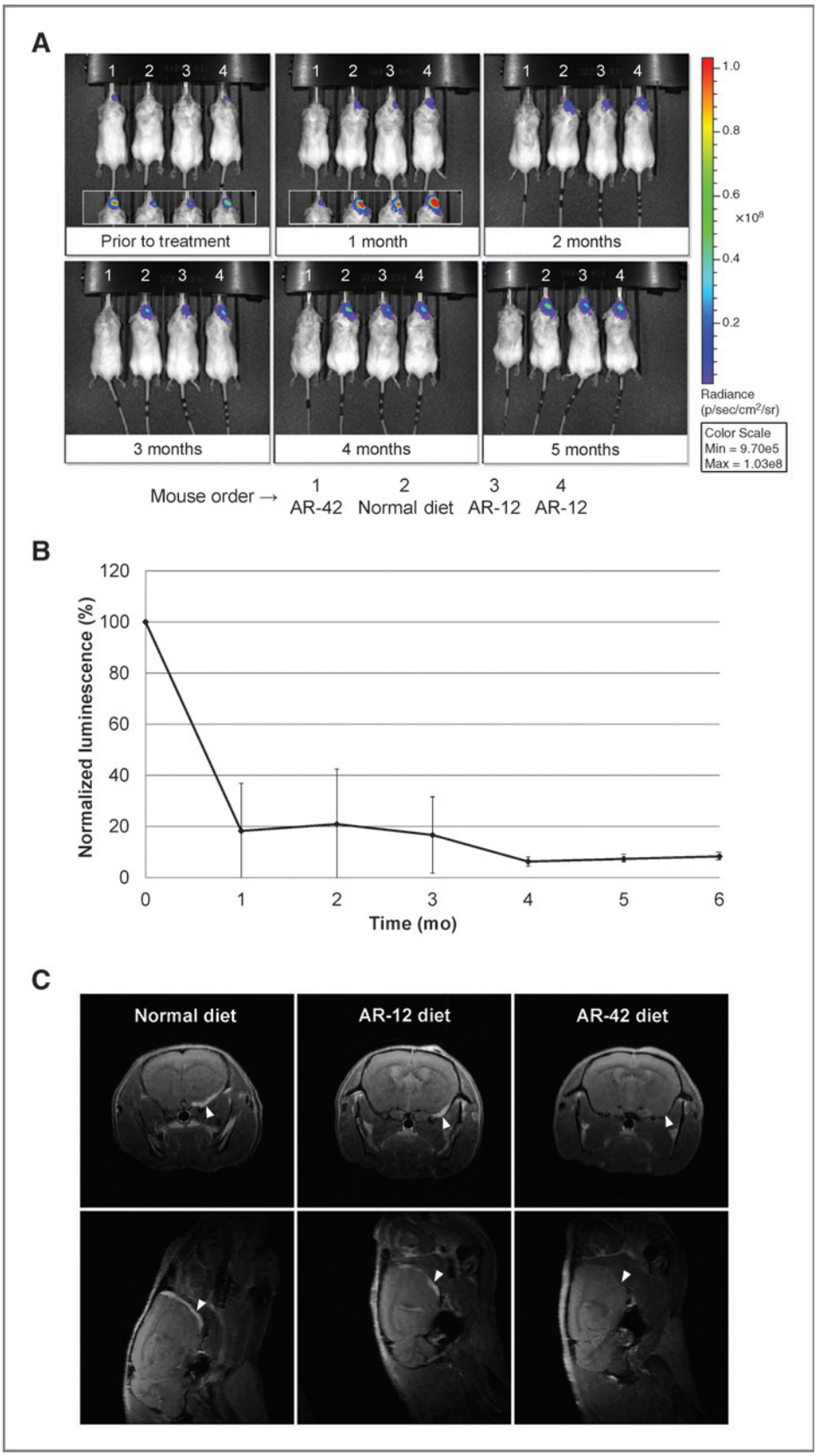

Figure 5. AR-42 potently suppressed the growth of Ben-Men-1-LucB tumor xenografts. Mice bearing Ben-Men-1-LucB tumors were established as described in Materials and Methods and fed either normal diet (mouse #2) or chow formulated with AR-42 (mouse #1) or AR-12 (mouse #3 and #4) for the indicated times ($n = 5$). Tumor growth was monitored by BLI. A, a representative image shows that while the intensity of bioluminescent signal increased over time in the mouse fed normal diet (mouse #2), the signal in the mouse fed AR-42 diet (mouse #1) decreased sharply after 1 month of treatment and remained low in subsequent months. The bioluminescent signal in mice treated with AR-12 (mouse #3 and #4) increased over time but at a slower rate than that in the mouse fed normal diet (mouse #2). Insets in the images of mice before and 1 month after treatment are displayed using a lower threshold of bioluminescence detection. B, quantitation of the bioluminescent signals emitted from tumors in mice fed AR-42–containing diet was conducted, and the relative bioluminescence signal is denoted as the percentage of total flux after each month of treatment relative to the total flux before treatment designated as a 100%. The data are shown as mean ± SD and reflect the BLI measurements from 5 animals per group imaged for 6 months. C, following BLI, tumor-bearing mice fed normal diet or diet containing AR-42 or AR-12 were imaged with gadolinium contrast using a small-animal MRI. Coronal (top) and axial (bottom) T1 MR images showed that the AR-12–treated mouse exhibited a smaller tumor than the mouse fed normal diet. Also, a tumor was not detected in the AR-42–treated mouse after 4 months of treatment. Arrowheads point to the site of injection at the skull base.

Published OnlineFirst November 14, 2012; DOI: 10.1158/0008-5472.CAN-12-1888

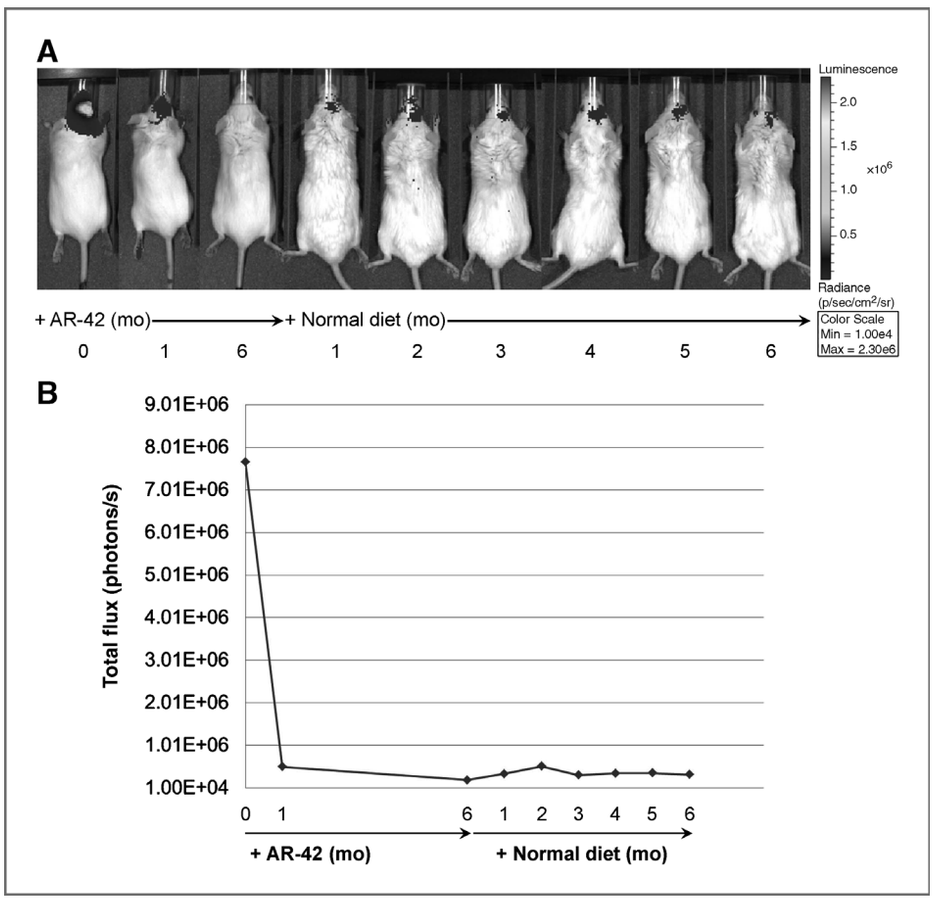

Figure 6. AR-42–treated tumors exhibited minimal regrowth. A Ben-Men-1-LucB xenograft–bearing mouse was fed AR-42 diet for 6 months and then switched to normal diet for an additional 6 months. A, the bioluminescence signal emitted from the tumor markedly decreased following AR-42 treatment and remained low with minimal regrowth after removal from AR-42 diet. B, quantitation of the bioluminescence intensity confirmed minimal tumor regrowth in the AR-42–treated mouse after switching to normal diet for 6 months.

Minimal regrowth of Ben-Men-1-LucB tumors was observed after removal from AR-42 treatment

To evaluate potential tumor regrowth following AR-42 treatment, we fed an AR-42–treated mouse normal diet for an additional 6 months and monitored tumor growth monthly by BLI. While AR-42 treatment substantially decreased the tumor size as shown by the marked decrease of bioluminescence signal after six months (from 7.7×10^6 to 2.0×10^5 photons/sec), the tumor remained small with minimal regrowth (~2-fold increase in bioluminescence signal) over 6 months after removal from AR-42–containing diet (Fig. 6). Also, the tumor remained too small to be detected by MRI (Supplementary Fig. S10).

Histologic analysis corroborated that the tumors in mice treated with AR-12 for 6 months were smaller than those fed normal diet (Fig. 7A). Also, a very small tumor was found in a mouse treated with AR-42 for 3 months, consistent with the MRI result. AR-42–treated tumors exhibited increased levels of acetylated proteins compared with mice fed normal diet or diet containing AR-12 (Fig. 7B). As observed in cultured cells (Fig. 3A), a higher level of $p16^{INK4A}$ was detected in the tumors of AR-42–treated mice than in those of mice fed normal diet (Supplementary Fig. S8B). Consistent with the potent growth-inhibitory activity of AR-42, few or no BrdUrd- or Ki67-positive cells were seen in AR-42–treated tumors. Together with our previous observation that AR-42 induces apoptosis *in vivo* (22), these results indicate that AR-42 efficiently inhibits tumor growth in the Ben-Men-1-LucB benign meningioma model.

Discussion

Development of novel therapeutics for meningiomas, particularly those associated with NF2, is urgently needed and requires disease-specific models. In the present study, we generated a quantifiable orthotopic *NF2*-deficient benign meningioma model using luciferase-expressing Ben-Men-1-LucB cells. Using this model, we compared the *in vivo* efficacies of AR-42, a pan-HDACi (25), and AR-12, a PDK1 inhibitor (37), and showed that AR-42 causes tumor regression, whereas AR-12 moderately slows the growth of tumors over time.

Previously, we reported that AR-42 efficiently inhibits schwannoma and meningioma cell proliferation by arresting cells at G_2–M and inducing apoptosis (22). Intriguingly, AR-42 inhibited proliferation of normal meningeal cells at about the same IC_{50} as that for Ben-Men-1 meningioma cells. Although AR-42 exerted similar effects on protein acetylation and AKT phosphorylation in both normal and tumor cells, it arrested meningeal cells at G_1 but inhibited Ben-Men-1 cells at both G_1 and G_2–M. Cell-cycle progression is modulated by CDKs, which are bound and activated by one or more cyclin proteins whose

Published OnlineFirst November 14, 2012; DOI: 10.1158/0008-5472.CAN-12-1888

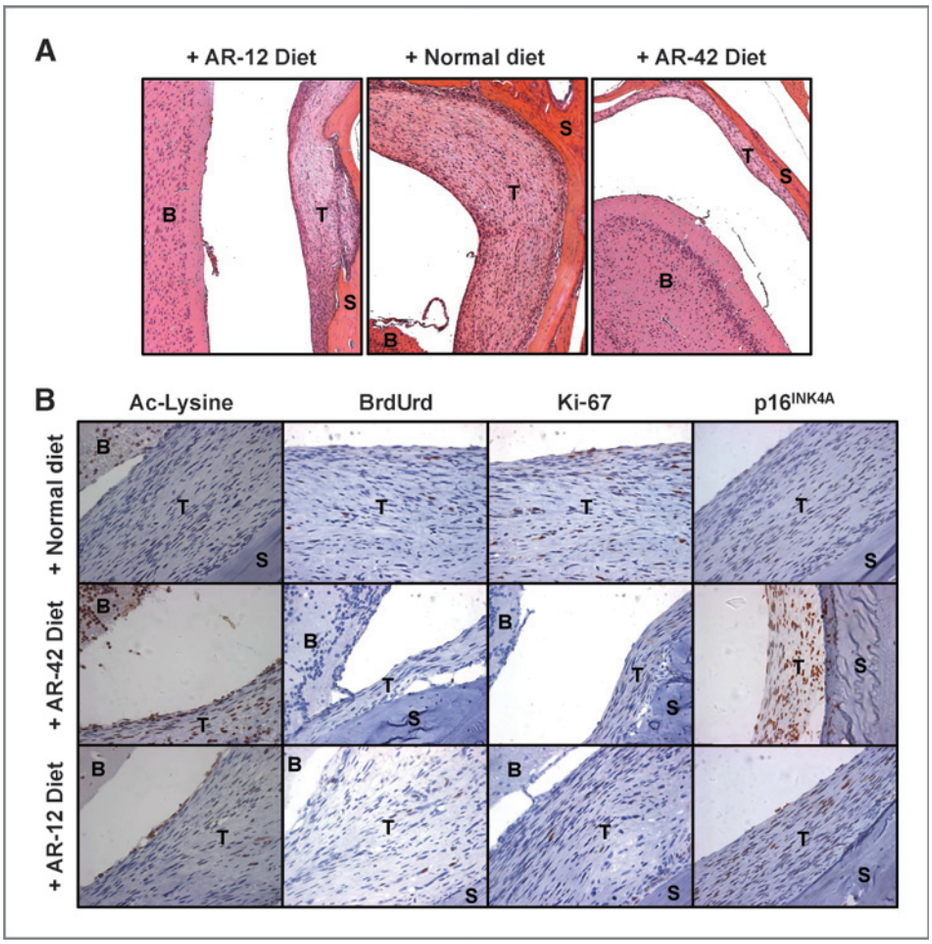

Figure 7. AR-42–treated tumors showed high levels of acetylated proteins and $p16^{INK4A}$. A, images shown are hematoxylin and eosin–stained sections from tumor-bearing mice fed normal diet or diet containing AR-12 for 6 months or fed AR-42–containing diet for 3 months. B, sections were immunostained for acetylated lysine (Ac-Lysine), BrdUrd, Ki67, and $p16^{INK4A}$. B, brain; T, tumor; S, skull.

expression oscillates during specific phases of the cell cycle (33). In addition, several regulatory checkpoints exist throughout the cell cycle to maintain genomic stability. Activation of the G_1 and G_2 checkpoints increases the expression of CDK inhibitors and arrests cells in these phases, providing them time to repair any damage before continuing the cell cycle (38). The INK4 family of CDK inhibitors inhibits cyclin D–associated CDK4/6 at G_1, whereas the CIP/KIP family regulates a wider range of cyclin–CDK complexes throughout the cell cycle. HDACi have been shown to induce G_1 and/or G_2–M arrest in tumor cells, and their action is mediated, in part, by altering the levels of various CDK inhibitors (39). HDACi can affect transcription of the $p16^{INK4A}$ and $p21^{CIP1/WAF1}$ genes and alter the $p27^{KIP1}$ level by a posttranslational mechanism. Consistently, AR-42 induced the expression of both the INK ($p16^{INK4A}$) and CIP/KIP ($p21^{CIP1/WAF1}$ and $p27^{KIP1}$) members. However, the induction of these CDK inhibitors by AR-42 in both meningeal and Ben-Men-1 meningioma cells implies that additional mechanisms contribute to the differential effects on cell-cycle progression in these cells.

Tumor cells frequently exhibit an abnormal G_1 checkpoint as evident by alteration of the G1 cyclin-CDKs/the INK family/the retinoblastoma protein/E2F cascade (33, 38). Consistent with this notion, Ben-Men-1 cells expressed higher basal levels of the G_1 cyclins, D1 and E, than meningeal cells. While AR-42 treatment decreased cyclin E and A expression, significant amounts of these cyclins and PCNA were still detected even in the presence of 2 μmol/L AR-42, suggesting that a fraction of AR-42–treated meningioma cells enter S-phase. It is possible that the increased expression of multiple CDK inhibitors, together with the decreased levels of G_1 cyclins, led to the growth inhibition at G_1 observed in AR-42–treated Ben-Men-1 cells. However, the reduction of cyclin B expression by AR-42 may further inhibit the Ben-Men-1 cells that had progressed through S-phase and arrest them at G_2. In contrast, AR-42 treatment blocked the expression of cyclin D1, E, and A in meningeal cells, and this inhibition, together with the elevated levels of CDK inhibitors, could explain the G_1 arrest observed in these cells. Consistently, only a small amount of PCNA and little cyclin B were detected in AR-42–treated meningeal cells. HDACi can affect cyclin D, E, and B expression through a transcriptional mechanism or increase acetylation of cyclin A, which facilitates its degradation (39–42). It will be interesting to investigate why AR-42 treatment caused a more pronounced reduction of the cyclin A level in meningeal cells than Ben-Men-1 cells. Nevertheless, the differential effect of AR-42 on cell-cycle progression of meningeal and meningioma cells involves modulation of the expression of multiple cell-cycle regulators.

Published OnlineFirst November 14, 2012; DOI: 10.1158/0008-5472.CAN-12-1888

The mitotic spindle assembly checkpoint, which protects the integrity of cell division, is frequently altered in human tumors and regulated by several kinases, including Bub1, Bub3, and BubR1 (34). In addition, Aurora kinases A and B are important for spindle assembly, chromosome segregation, and cytokinesis (43). Curiously, Ben-Men-1 cells expressed higher levels of Aurora A, Aurora B, and BubR1 than meningeal cells, suggesting deregulation of the mitotic spindle checkpoint in meningioma cells. Importantly, AR-42 decreased the expression of Aurora A and B, further corroborating G_2–M arrest in Ben-Men-1 cells. HDACi can decrease transcription of Aurora A and B or promote their degradation in different cell types (44–45). However, the mechanism by which AR-42 reduces the expression of Aurora kinases in meningeal and meningioma cells is not known. As Aurora A and B are frequently amplified or overexpressed in a variety of solid and hematologic malignancies (34, 43), AR-42 may also be a potential therapeutic agent for these tumors.

The members of the Bcl2 family, which consists of proapoptotic and anti-apoptotic factors, interact with each other in a delicate balance that governs whether a cell will undergo apoptosis. Our observation that AR-42 increased the expression of Bim and Bag1 and decreased the level of Bcl_{XL} coincides with previous findings that AR-42 induced apoptosis in tumor cells (22, 32, 35, 36). Also, HDACi have been shown to induce the expression of Bcl2 family members, including Bim and Bcl_{XL} (35, 36, 46). Together, these results suggest that AR-42–induced apoptosis is mediated, in part, through modulation of proapoptotic and anti-apoptotic factors.

Previously, we (21) showed that AR-12, a derivative of celecoxib that lacks COX-2 inhibitory activity (37), decreased AKT phosphorylation and efficiently inhibited schwannoma growth *in vitro* and *in vivo*. As in schwannoma xenografts (21), AR-12 exhibited moderate antitumor activity in Ben-Men-1-LucB meningiomas. Interestingly, AR-42 gave rise to more profound growth inhibition than AR-12 and caused tumor regression, suggesting that inhibition of the AKT pathway is not sufficient to account for the antitumor potency of AR-42. Also, the residual tumors in AR-42-treated mice showed minimal regrowth after switching to normal diet. As AR-42 also potently inhibits schwannoma growth and is well tolerated in mice (22, 23), these results suggest that it is a promising therapeutic agent for *NF2*-deficient tumors.

BLI is a sensitive and efficient way to noninvasively monitor tumor growth, particularly for longitudinal studies of benign tumors. Using BLI, we detected bioluminescence signal emitted from small luciferase-expressing tumors in AR-42–treated mice, whereas MRI could not identify tumors in the same mice. This observation is consistent with a previous report that MRI efficiently identifies macroscopic tumors but is less effective at detecting small tumors in mice compared with BLI (47). Also, MRI measured a less pronounced reduction in tumor size in AR-12–treated mice than BLI. It is possible that BLI may quantify the differences in cell density in benign tumors. Treatment may affect peritumoral edema of intracranial meningiomas (48), and fluid surrounding the tumors may obscure the tumor margin used in volumetric MRI measurement. Nevertheless, MRI and BLI were complementary tools to quantify the effects of AR-42 and AR-12 on tumor growth.

Overexpressed or sustained HDAC activity has been observed in many solid and hematologic malignancies, suggesting therapeutic potential of HDACi (24, 49). Several HDACi are currently in clinical trials for various types of cancer. Among them, Zolinza (vorinostat) and Romidepsin (depsipeptide) have been approved by the U.S. Food and Drug Administration (FDA) for the treatment of cutaneous T-cell lymphomas. AR-42 possesses growth-inhibitory activity that is comparable to or more potent than vorinostat in several tumor models (32, 35, 36, 50). It is orally bioavailable, penetrates the blood–brain barrier, and exhibits low toxicity. Mice treated with AR-42 showed slight weight loss, leukopenia, anemia, liver hypertrophy, and testicular degeneration, and these effects are reversible after removal from treatment (23, 50). AR-42 is currently being evaluated in a phase I/IIa clinical trial for relapsed and refractory multiple myeloma, chronic lymphocytic leukemia, and lymphoma. Our observation that AR-42 differentially affects cell-cycle progression of normal meningeal and meningioma cells may have implications for why it is well-tolerated while potently inhibiting tumor growth as prolonged G_2 arrest may lead to apoptosis in proliferating tumor cells. Collectively, our results suggest that AR-42 merits a clinical trial for meningiomas and schwannomas.

Disclosure of Potential Conflicts of Interest

C.-S. Chen has ownership interest (including patents) and has royalty from licensing agreement between OSU and Arno. No potential conflicts of interest were disclosed by the other authors.

Authors' Contributions

Conception and design: S.S. Burns, M.L. Bush, C.-S. Chen, A. Jacob, D.B. Welling, L.-S. Chang
Development of methodology: S.S. Burns, E.M. Akhmametyeva, J.L. Oblinger, M.L. Bush, J. Huang, D.B. Welling, L.-S. Chang
Acquisition of data (provided animals, acquired and managed patients, provided facilities, etc.): S.S. Burns, A. Jacob, D.B. Welling, L.-S. Chang
Analysis and interpretation of data (e.g., statistical analysis, biostatistics, computational analysis): S.S. Burns, L.-S. Chang
Writing, review, and/or revision of the manuscript: S.S. Burns, M.L. Bush, A. Jacob, D.B. Welling, L.-S. Chang
Administrative, technical, or material support (i.e., reporting or organizing data, constructing databases): S.S. Burns, E.M. Akhmametyeva, J.L. Oblinger, M.L. Bush, J. Huang, V. Senner, C.-S. Chen, A. Jacob, L.-S. Chang
Study supervision: L.-S. Chang

Acknowledgments

The authors sincerely thank Anita Lal for KT21-MG1 and IOMM-Lee cells, Kimerly Powell and the Small-Animal Imaging Core for MRI, Allen Qian for technical assistance, and Beth Miles-Markley and Peter Houghton for critical reading of the manuscript.

Grant Support

This study was supported by grants from the Children's Tumor Foundation, NIDCD (DC005985), US Department of Defense (NF080021), NF Midwest, and Advocure NF2 to D.B. Welling and L.-S. Chang.

The costs of publication of this article were defrayed in part by the payment of page charges. This article must therefore be hereby marked *advertisement* in accordance with 18 U.S.C. Section 1734 solely to indicate this fact.

Received May 14, 2012; revised September 6, 2012; accepted October 25, 2012; published OnlineFirst November 14, 2012.

Published OnlineFirst November 14, 2012; DOI: 10.1158/0008-5472.CAN-12-1888

References

1. Wiemels J, Wrensch M, Claus EB. Epidemiology and etiology of meningioma. J Neurooncol 2010;99:307–14.
2. Goutagny S, Kalamarides M. Meningiomas and neurofibromatosis. J Neurooncol 2010;99:341–7.
3. Rouleau GA, Merel P, Lutchman M, Sanson M, Zucman J, Marineau C, et al. Alteration in a new gene encoding a putative membrane-organizing protein causes neuro-fibromatosis type 2. Nature 1993;363:515–21.
4. Trofatter JA, MacCollin MM, Rutter JL, Murrell JR, Duyao MP, Parry DM, et al. A novel moesin-, ezrin-, radixin-like gene is a candidate for the neurofibromatosis 2 tumor suppressor. Cell 1993;72:791–800.
5. James MF, Han S, Polizzano C, Plotkin SR, Manning BD, Stemmer-Rachamimov AO, et al. NF2/merlin is a novel negative regulator of mTOR complex 1, and activation of mTORC1 is associated with meningioma and schwannoma growth. Mol Cell Biol 2009;29:4250–61.
6. Kalamarides M, Niwa-Kawakita M, Leblois H, Abramowski V, Perricaudet M, Janin A, et al. *Nf2* gene inactivation in arachnoidal cells is rate-limiting for meningioma development in the mouse. Genes Dev 2002;16:1060–5.
7. Kalamarides M, Stemmer-Rachamimov AO, Niwa-Kawakita M, Chareyre F, Taranchon E, Han ZY, et al. Identification of a progenitor cell of origin capable of generating diverse meningioma histological subtypes. Oncogene 2011;30:2333–44.
8. Lee WH. Characterization of a newly established malignant meningioma cell line of the human brain: IOMM-Lee. Neurosurgery 1990;27:389–95.
9. Tanaka K, Sato C, Maeda Y, Koike M, Matsutani M, Yamada K, et al. Establishment of a human malignant meningioma cell line with amplified c-myc oncogene. Cancer 1989;64:2243–9.
10. Ragel BT, Elam IL, Gillespie DL, Flynn JR, Kelly DA, Mabey D, et al. A novel model of intracranial meningioma in mice using luciferase-expressing meningioma cells. J Neurosurg 2008;108:304–10.
11. McCutcheon IE, Friend KE, Gerdes TM, Zhang BM, Wildrick DM, Fuller GN. Intracranial injection of human meningioma cells in athymic mice: an orthotopic model for meningioma growth. J Neurosurg 2000;92:306–14.
12. Baia GS, Dinca EB, Ozawa T, Kimura ET, McDermott MW, James CD, et al. An orthotopic skull base model of malignant meningioma. Brain Pathol 2008;18:172–9.
13. Cargioli TG, Ugur HC, Ramakrishna N, Chan J, Black PM, Carroll RS. Establishment of an *in vivo* meningioma model with human telomerase reverse transcriptase. Neurosurgery 2007;60:750–9.
14. Baia GS, Slocum AL, Hyer JD, Misra A, Sehati N, VandenBerg SR, et al. A genetic strategy to overcome the senescence of primary meningioma cell cultures. J Neurooncol 2006;78:113–21.
15. Püttmann S, Senner V, Braune V, Hillmann B, Exeler R, Rickert C, et al. Establishment of a benign meningioma cell line by hTERT-mediated immortalization. Lab Invest 2005;85:1163–71.
16. Watson MA, Gutmann DH, Peterson K, Chicoine MR, Kleinschmidt-DeMasters BK, Brown HG, et al. Molecular characterization of human meningiomas by gene expression profiling using high density oligonucleotide microarrays. Am J Pathol 2002;161:665–72.
17. Welling DB, Lasak JM, Akhmametyeva E, Ghaheri B, Chang LS. cDNA microarray analysis of vestibular schwannomas. Otol Neurotol 2002;23:736–48.
18. Cuevas IC, Slocum AL, Jun P, Costello JF, Bollen AW, Riggins GJ, et al. Meningioma transcript profiles reveal deregulated Notch signaling pathway. Cancer Res 2005;65:5070–5.
19. Hanemann CO, Bartelt-Kirbach B, Diebold R, Kämpchen K, Langmesser S, Utermark T. Differential gene expression between human schwannoma and control Schwann cells. Neuropathol Appl Neurobiol 2006;32:605e14.
20. Jacob A, Lee TX, Neff BA, Miller S, Welling B, Chang L-S. Phosphatidylinositol 3-kinase/AKT pathway activation in human vestibular schwannoma. Otol Neurotol 2008;29:58–68.
21. Lee TX, Packer MD, Huang J, Akhmametyeva EM, Kulp SK, Chen C-S, et al. Growth inhibitory and anti-tumor activities of OSU-03012, a novel PDK-1 inhibitor, on vestibular schwannoma and malignant schwannoma cells. Eur J Cancer 2009;45:1709–20.
22. Bush ML, Oblinger J, Brendel V, Santarelli G, Huang J, Akhmametyeva EM, et al. AR42, a novel histone deacetylase inhibitor, as a potential therapy for vestibular schwannomas and meningiomas. Neuro Oncol 2011;13:983–99.
23. Jacob A, Oblinger J, Bush ML, Brendel V, Santarelli G, Ray-Chaudhury A, et al. Preclinical validation of AR42, a novel histone deacetylase inhibitor, as treatment for vestibular schwannomas. Laryngoscope 2012;122:174–89.
24. Minucci S, Pelicci PG. Histone deacetylase inhibitors and the promise of epigenetic (and more) treatments for cancer. Nat Rev Cancer 2006;6:38–51.
25. Chen CS, Weng SC, Tseng PH, Lin HP, Chen C-S. Histone acetylation-independent effect of histone deacetylase inhibitors on Akt through the reshuffling of protein phosphatase 1 complexes. J Biol Chem 2005;280:38879–87.
26. Chang L-S, Jacob A, Lorenz M, Rock J, Akhmametyeva EM, Mihai G, et al. Growth of benign and malignant schwannoma xenografts in severe combined immunodeficiency mice. Laryngoscope 2006;116:2018–26.
27. Chang L-S, Welling DB. Molecular biology of vestibular schwannomas. Methods Mol Biol 2009;493:163–77.
28. Fields RD, Lancaster MV. Dual attribute continuous monitoring of cell proliferation/cytotoxicity. Am Biotechnol Lab 1993;11:48–50.
29. Darzynkiewicz Z, Juan G. DNA content measurement for DNA ploidy and cell cycle analysis. In Current protocols in flow. Somerset, NJ: John Wiley & Sons, Inc.; 1997. Unit 7.5.
30. Chang L-S, Akhmametyeva EM, Wu Y, Zhu L, Welling DB. Multiple transcription initiation sites, alternative splicing, and differential polyadenylation contribute to the complexity of human neurofibromatosis 2 transcripts. Genomics 2002;79:63–76.
31. Seilly DJ. A chemical test to determine the end point of EDTA decalcification. Med Lab Sci 1982;39:71–3.
32. Yang YT, Balch C, Kulp SK, Mand MR, Nephew KP, Chen CS. A rationally designed histone deacetylase inhibitor with distinct antitumor activity against ovarian cancer. Neoplasia 2009;11:552–63.
33. Hochegger H, Takeda S, Hunt T. Cyclin-dependent kinases and cell-cycle transitions: does one fit all. Nat Rev Mol Cell Biol 2008;9:910–6.
34. Kops GJ, Weaver BA, Cleveland DW. On the road to cancer: aneuploidy and the mitotic checkpoint. Nat Rev Cancer 2005;5:773–85.
35. Kulp SK, Chen CS, Wang DS, Chen CY, Chen CS. Antitumor effects of a novel phenylbutyrate-based histone deacetylase inhibitor, (S)-HDAC-42, in prostate cancer. Clin Cancer Res 2006;12:5199–206.
36. Lu YS, Kashida Y, Kulp SK, Wang YC, Wang D, Hung JH, et al. Efficacy of a novel histone deacetylase inhibitor in murine models of hepatocellular carcinoma. Hepatology 2007;46:1119–30.
37. Zhu J, Huang JW, Tseng PH, Yang YT, Fowble J, Shiau CW, et al. From the cyclooxygenase-2 inhibitor celecoxib to a novel class of 3-phosphoinositide-dependent protein kinase-1 inhibitors. Cancer Res 2004;64:4309–18.
38. Sherr CJ, Roberts JM. CDK inhibitors: positive and negative regulators of G1-phase progression. Genes Dev 1999;13:1501–12.
39. Mork CN, Faller DV, Spanjaard RA. A mechanistic approach to anticancer therapy: targeting the cell cycle with histone deacetylase inhibitors. Curr Pharm Des 2005;11:1091–104.
40. Nair AR, Boersma LJ, Schiltz L, Chaudhry MA, Muschel RJ. Paradoxical effects of trichostatin A: inhibition of NF-Y-associated histone acetyltransferase activity, phosphorylation of hGCN5 and downregulation of cyclin A and B1 mRNA. Cancer Lett 2001;166:55–64.
41. Sambucetti LC, Fischer DD, Zabludoff S, Kwon PO, Chamberlin H, Trogani N, et al. Histone deacetylase inhibition selectively alters the activity and expression of cell cycle proteins leading to specific chromatin acetylation and antiproliferative effects. J Biol Chem 1999;274:34940–47.
42. Mateo F, Vidal-Laliena M, Canela N, Busino L, Martinez-Balbas MA, Pagano M, et al. Degradation of cyclin A is regulated by acetylation. Oncogene 2009;28:2654–66.

Published OnlineFirst November 14, 2012; DOI: 10.1158/0008-5472.CAN-12-1888

43. Keen N, Taylor S. Aurora-kinase inhibitors as anticancer agents. Nat Rev Cancer 2004;4:927–36.

44. Li Y, Kao GD, Garcia BA, Shabanowitz J, Hunt DF, Qin J, et al. A novel histone deacetylase pathway regulates mitosis by modulating Aurora B kinase activity. Genes Dev 2006;20:2566–79.

45. Cha TL, Chuang MJ, Wu ST, Sun GH, Chang SY, Yu DS, et al. Dual degradation of aurora A and B kinases by the histone deacetylase inhibitor LBH589 induces G2-M arrest and apoptosis of renal cancer cells. Clin Cancer Res 2009;15:840–50.

46. Zhao Y, Tan J, Zhuang L, Jiang X, Liu ET, Yu Q. Inhibitors of histone deacetylases target the Rb-E2F1 pathway for apoptosis induction through activation of proapoptotic protein Bim. Proc Natl Acad Sci USA 2005;102:16090–95.

47. Puaux AL, Ong LC, Jin Y, Teh I, Hong M, Chow PK, et al. A comparison of imaging techniques to monitor tumor growth and cancer progression in living animals. Int J Mol Imaging 2011; e321538.

48. Nakano T, Asano K, Miura H, Itoh S, Suzuki S. Meningiomas with brain edema: radiological characteristics on MRI and review of the literature. Clin Imaging 2002;26:243–9.

49. Bolden JE, Peart MJ, Johnstone RW. Anticancer activities of histone deacetylase inhibitors. Nat Rev Drug Discov 2006;5:769–84.

50. Sargeant AM, Rengel RC, Kulp SK, Klein RD, Clinton SK, Wang YC, et al. OSU-HDAC42, a histone deacetylase inhibitor, blocks prostate tumor progression in the transgenic adenocarcinoma of the mouse prostate model. Cancer Res 2008;68:3999–4009.